Electronic Coherence and Collective Optical Excitations of Conjugated Molecules

Shaul Mukamel,* Sergei Tretiak, Thomas Wagersreiter, Vladimir Chernyak

Optical spectroscopy of conjugated molecules is described by using collective electronic coordinates, which represent the joint dynamics of electron-hole pairs. The approach relates the optical signals directly to the dynamics of charges and bond orders (electronic coherences) induced by the radiation field and uses only ground-state information, thus avoiding the explicit calculation of excited molecular states. The resulting real-space picture is reminiscent of the normal-mode analysis of molecular vibrations and offers a unified framework for the treatment of other types of systems including semiconductor nanostructures and biological complexes. Spatial coherence displayed in two-dimensional plots of the five electronic normal modes that dominate the optical response of poly(*p*-phenylene vinylene) oligomers with up to 50 repeat units (398 carbon atoms) in the 1.5- to 8-electronvolt frequency range suggests a saturation to bulk behavior at about five repeat units.

Spectroscopy allows chemists and physicists to probe of the dynamics of vibrations and electronic excitations within molecules and solids. The theoretical models used for interpreting molecular spectra compared with those for extended solids are usually quite different, and certain systems, such as clusters and polymers, are not readily treated by either of these limiting cases. There is particular interest to understand the optical spectra of large polymers, which are extended conjugated molecules such as poly(*p*-phenylene vinylene) (PPV) oligomers (Fig. 1) that have interesting optical applications.

Electronic and optical properties of small conjugated chains can be interpreted molecularly in terms of their global many-electron eigenstates obtained from quantum-chemistry methods (*1*, *2*). Large polymers also can be analyzed with semiconductor band theories that focus on the dynamics of electron-hole pairs (*3*). The size-scaling of the optical response and the transition between these two regimes has not been fully explored for the lack of adequate theoretical methods. It is very hard to obtain the complete set of eigenstates, which carry considerably more information than necessary for the calculation of spectra, for large molecules with strong electron correlations (as occurs in conjugated chains). Band theories, however, neglect electronic correlation effects, and because they are formulated in momentum (k) space, they do not lend themselves easily to real-space chemical intuition.

The collective-electronic oscillator (CEO) representation (*4*, *5*) provides a hybrid formulation that bridges the gap between the chemical and semiconductor points of view. This model uses an electron-hole picture in real space, overcomes many of the difficulties associated with the former approaches, and provides a physically intuitive link between electronic structure and optical properties, that is, the optical properties are related directly to the motions of charges and electronic coherences, thus avoiding the need to calculate the global (many-electron) eigenstates. The electronic oscillators, unlike the electronic orbitals, are directly observable spectroscopically (*4*–*6*). Despite the quantum nature of electronic motions, the collective oscillators are classical (*7*, *8*), which relates well with chemical intuition. Typically only a few oscillators dominate the response, greatly simplifying the theoretical description. A real-space picture of linear absorption that pinpoints the origin of each optical transition is obtained by two-dimensional (2D) display of the electronic mode matrices. Our results provide a unified description of the optical response of small and large molecules as well as bulk materials.

The authors are in the Department of Chemistry and the Rochester Theory Center for Optical Science and Engineering, University of Rochester, Rochester, NY 14627, USA.

*To whom correspondence should be addressed.

The CEO Approach

The oscillator picture that we use here is more familiar in the analysis of vibrational spectroscopy (*9*), in which the coherent motions of various atoms with well-defined amplitude and phase relations are represented by collective nuclear coordinates—the normal modes. The normal modes provide a natural coordinate system and allow an alternative classical real-space interpretation of infrared or Raman spectra (*9*, *10*) instead of a description in terms of transitions among specific vibrational states. The normal modes of nuclear vibrations are simply superpositions of the $3N$ nuclear displacements. Extending this concept to electronic motions is not straightforward, however, because spectroscopic observables are highly averaged, and following the complete many-electron dynamics is neither feasible nor desirable. For this reason, the oscillator picture is normally not used for electronic spectroscopy.

In this article we show how a CEO picture can be rigorously established for optical excitations of conjugated molecules. We demonstrate how a natural set of electronic coordinates can be constructed by using the reduced single-electron density matrix (*4*, *5*, *11*) and how it offers tremendous conceptual as well as computational advantages. Consider a conjugated molecule described by a basis set $\{\phi_n\}$ of N atomic orbitals. [For simplicity we use in the calculations presented below the Pariser-Parr-Pople (PPP) Hamiltonian where each carbon atom has a single π orbital (*6*, *12*). N then coincides with the number of carbon atoms.] The system can be described by the Fermi operators c_n^+ and c_n representing the creation and annihilation, respectively, of an electron in ϕ_n. The complete many-electron wave function representing the system's ground state will be denoted $\psi_g(\mathbf{x})$, $\mathbf{x}$ being the complete set of electronic coordinates. The reduced single-electron ground-state density matrix is then defined as the expectation value (*13*)

$$\bar{\rho}_{nm} \equiv \langle \psi_g | c_n^+ c_m | \psi_g \rangle \qquad (1)$$

(Spin indices have been omitted for brevity.) The physical significance of $\bar{\rho}$ has been recognized since the early days of quantum chemistry (*14*). We first note that $\bar{\rho}$ is an $N \times N$ matrix. The density matrix carries considerably less information than the complete many-electron wave function (making it much easier to calculate); however, this information is sufficient to calculate all op-

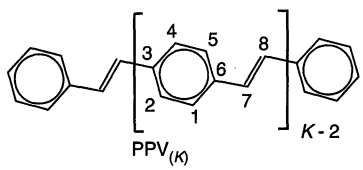

Fig. 1. Geometry and atom labeling of PPV oligomers. Bond angles are 120°, except $\alpha(r_{6,7}, r_{7,8}) = 128°$, and the distances are $r_{1,2} = r_{2,3} = r_{3,4} = r_{4,5} = r_{5,6} = r_{6,1} = 1.39$ Å, $r_{6,7} = 1.44$ Å, and $r_{7,8} = 1.33$ Å.

tical properties and develop an intuitive physical picture of the optical response. [$\psi_g(\mathbf{x})$ allows us to calculate the expectation values of products of arbitrary numbers of c_n at c_n^+, whereas $\bar{\rho}$ only gives the binary products, which represent operators that depend on a single electron, hence its name.] $\bar{\rho}$ is thus the quantum analog of the single-particle distribution in classical statistical mechanics (*15*). The ground-state density matrix $\bar{\rho}_{nm}$ may be obtained by using standard quantum chemistry packages. Its diagonal elements ($n = m$) represent the charge at the mth atom, whereas the off-diagonal elements ($n \neq m$) reflect the strength of chemical bonding between each pair of atoms and are known as the bond orders. Bond order is thus associated with a phase relation (electronic coherence) between orbitals. The eigenvectors of $\bar{\rho}$ known as the natural orbitals provide a convenient basis set for performing configuration interaction calculations and for interpreting chemical reactivity (*16*, *17*).

When the molecule is driven by an external electric field (such as provided by a photon in a spectroscopic measurement), its wave function (and consequently, the reduced density matrix) becomes time-dependent, such that $\rho(t) = \bar{\rho} + \delta\rho(t)$. The matrix elements $\delta\rho_{nm}(t)$ represent the changes induced in the density matrix by the electric field. $\delta\rho_{nn}(t)$ is the net charge induced on the nth atom, whereas $\delta\rho_{nm}(t)$, $n \neq m$, is a dynamical bond order representing the joint amplitude of finding an electron on atom m and a hole on atom n.

Quantum chemistry techniques that calculate properties such as polarizabilities by using the many-body wave functions rapidly become more complicated with molecular size and are therefore limited to small molecules. Furthermore, in most practical chemical applications we need much less information than is carried by the complete eigenstates. This makes it hard to develop a simple intuitive understanding of various trends. A time-dependent procedure for calculating $\delta\rho(t)$ directly for a molecule interacting with an external electric field $\varepsilon(t)$ can be obtained by starting with the Heisenberg equation of motion for $c_n^+ c_m$. This equation is not closed, because higher order products will show up when the time derivative is calculated. Writing equations of motion for these higher order products will yield increasingly higher order products. This is the famous hierarchy of many-body (classical and quantum) dynamics. To overcome this difficulty we need a truncation procedure. The simplest procedure assumes that the many-body wave function is given by a single Slater determinant at all times and yields the time-dependent Hartree-Fock (TDHF) equations of motion (*18*):

$$\delta\dot{\rho} = A\delta\rho + B\delta\rho\delta\rho - \varepsilon(t)\mu\delta\rho \quad (2)$$

The coefficients (A, B, and μ) in these equations are readily available and depend on the original Hamiltonian and on $\bar{\rho}$ (which is the essential input in the present approach). Figure 2 displays $\bar{\rho}$ of a linear 30-atom polyacetylene chain as well as the induced density matrix $\delta\rho(\omega)$ [the Fourier transform of $\delta\rho(t)$] to first order in the external field [$\varepsilon(t)$], for three frequencies corresponding to the lowest peaks in the optical absorption. $\bar{\rho}$ is almost diagonal; only nearest neighbors have significant off-diagonal elements. This result is in agreement with our elementary picture of chemical bonding. Optical excitations, however, induce electronic coherences between atoms that are much farther apart, as is clearly seen in Fig. 2, B, C, and D.

With Eq. 2 the time-dependent density matrix (and optical excitations) can be calculated directly from $\bar{\rho}$. By understanding the mechanism for the creation of the coherence, we can develop a new type of chemical intuition and relate the optical response directly to the motions of charges and bond orders. This is an attractive alternative to the conventional description of spectra in terms of transitions among eigenstates. Both pictures are correct, and for historical reasons, chemical intuition is traditionally based on eigenstates. However, we argue that the real-space picture is much more natural, intuitive, and easier to implement once the proper terminology is developed. To illustrate this point, consider the variation of optical properties such as the electronic band gap and its oscillator strength or the magnitude of the off-resonant polarizability with molecular size. These properties strongly depend on size for short chains and level off at about 20 to 30 double bonds, where they attain the bulk values (*19*). It is impossible to visualize this coherence size by examining the molecular orbitals. These orbitals are completely delocalized, change gradually and continuously with chain length, and contain no signatures of this coherence size. In contrast, by looking at the induced density matrix one can immediately note the coherence size associated with its off-diago-

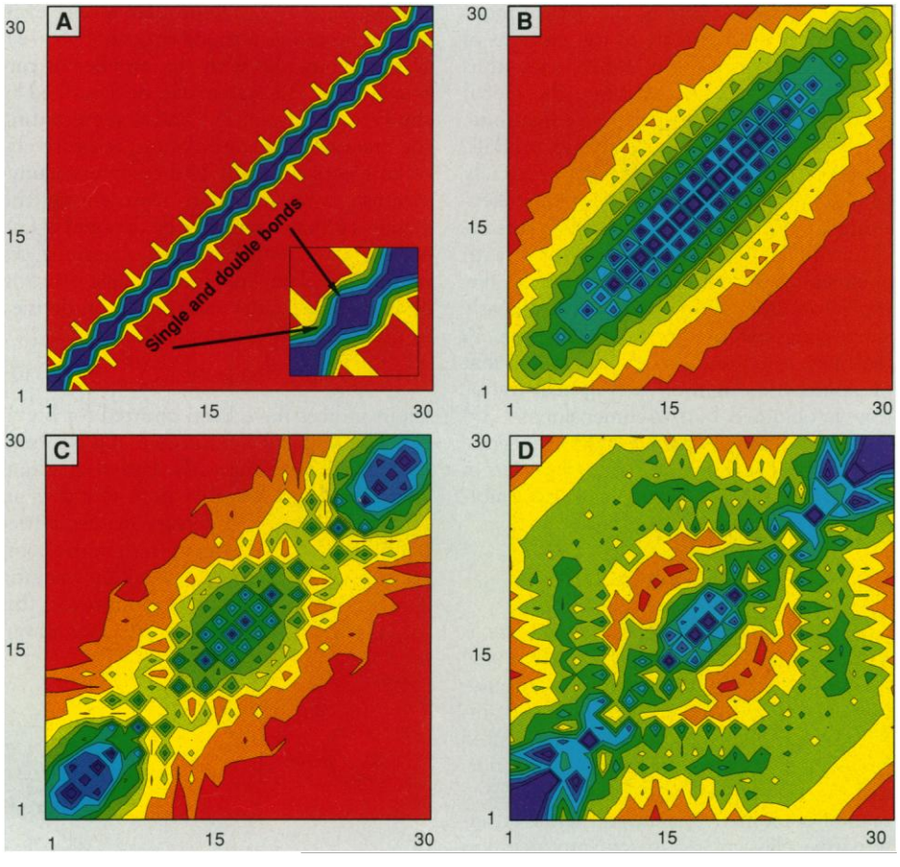

Fig. 2. Contour plots of density matrices of a 30-carbon polyacetylene chain. (**A**) Ground-state density matrix $\bar{\rho}$; (**B**, **C**, and **D**) frequency-dependent density matrices $\delta\rho(\omega)$ at ω = 2.5, 3.5, and 4.7 eV (496, 354, and 264 nm) corresponding to the lowest three dominant peaks in the absorption spectrum. The axes represent the individual carbon atoms, and the color code is shown in Fig. 4.

nal section. This coherence size, which measures how far apart different atoms communicate, controls the scaling of optical properties with size, as will be demonstrated below.

At this point, we return to the analogy with classical molecular vibrations. The displacements of nuclear positions from their equilibrium values satisfy nonlinear equations of motion resulting from the anharmonic force fields. Infrared and Raman spectra are usually interpreted by using normal modes obtained by diagonalizing the linear (harmonic) part of these equations of motion. Normal modes are natural collective coordinates for atomic displacements. Nonlinear (anharmonic) effects can be treated as perturbations. In complete analogy, $\delta\rho_{nm}(t)$ represent the displacements of the electronic density matrix elements from their equilibrium (ground state) values $\bar{\rho}_{nm}$. The nonlinear TDHF equations are the electronic counterpart of the classical Newtons' equations of motion of nuclear displacements. By diagonalizing the linearized TDHF equations, we obtain a set of collective electronic normal modes. The induced density matrix can then be expanded as a superposition of these collective modes in the same way that an atomic nuclear displacement is a superposition of the vibrational normal modes. Each normal mode (electronic oscillator) with frequency Ω_ν is described by a coordinate Q_ν and momentum P_ν. Q_ν and P_ν are also $N \times N$ matrices (*5*). These $N^2/4$ coordinates and momenta allow us to represent the time-dependent density matrix in the form (*4*)

$$\delta\rho(t) = \sum_{\nu=1}^{N^2/4} a_\nu(t)Q_\nu + b_\nu(t)P_\nu \qquad (3)$$

The time-dependent coefficients a_ν and b_ν are obtained by solving the TDHF equations.

The optical polarization is related to the charge distribution and may be expressed in terms of the diagonal elements of $\delta\rho(t)$. The polarization along the z axis is given by

$$\langle \mathcal{P}(t) \rangle = \sum e z_n \, \delta\rho_{nn}(t) \qquad (4)$$

where z_n is the z coordinate of the nth atom, and e is the electronic charge.

In the CEO method (*4*, *5*), the N^2 matrix elements of $\delta\rho(t)$ are obtained by solving the closed nonlinear TDHF equations of motion (*4*). These equations map the calculation of the optical response onto the dynamics of coupled electronic oscillators (analogous to calculating molecular vibrations), thus avoiding the tedious calculation of the global (many-electron) wave functions. Infrared and Raman spectra are greatly simplified by selection rules that allow us to include only a few modes in the calculation. The same is true for the electronic normal modes: Only a few dominant modes typically determine the spectra, thus greatly simplifying the physical picture and reducing the computational effort.

2D Real-Space Analysis of Optical Responses

We investigated the electronic excitations of PPV oligomers (Fig. 1) (*6*, *20*–*27*) and analyzed their scaling with size. Recent interest in PPV is connected with its possible use as a photoconductor (*28*, *29*), as a candidate for electroluminescent devices, or for optical switches.

The π molecular orbitals of PPV have been classified as either localized (l) or delocalized (d) (*26*, *28*). The former have an electron density on carbon atoms 1, 2, 4, and 5 (Fig. 1), whereas the latter are delocalized over all carbon atoms. The experimental absorption spectrum of PPV thin film (*21*) shown in Fig. 3A (dashed line) is typical for other PPV derivatives (*21*, *25*, *28*). It has a fundamental ($d \rightarrow d^*$) band at 2.5 eV (496 nm) (I), two weak peaks at 3.7 eV (335 nm) ($d \rightarrow d^*$) (II) and 4.8 eV (258 nm) ($l \rightarrow$ d* and $d \rightarrow l^*$) (III), and a strong ($l \rightarrow l^*$) band at 6.0 eV (207 nm) (IV). Peak II originates from electron correlations (*26*, *28*) and is missed by HF calculations. The calculated spectrum of $PPV_{(10)}$ shown in Fig. 3A (solid line) closely resembles the experimental spectrum and has similar features at 2.83 (I), 3.3 (II), 4.5 (III), and 5.6 eV (IV) (438, 376, 276, and 221 nm). In addition, it shows a fifth band centered at 7.0 eV (177 nm) (V). The oscillator strengths f_ν of $PPV_{(10)}$ are shown in Fig. 3A.

By displaying the dominant oscillators in the site representation, we obtain a new picture that relates the optical properties directly to motions of charges in the system, without introducing electronic eigenstates. The extent of spatial coherence then provides a view of the underlying coherence sizes. A 2D plot of $\bar{\rho}$ of $PPV_{(10)}$ is shown in Fig. 4A. The coordinate axes represent repeat units along the chain, and the absolute values of matrix elements are depicted by different colors. Similar to Fig. 2, $\bar{\rho}$ is dominated by the diagonal and near-diagonal elements, reflecting the bonds between nearest neighbors. A single unit of Fig. 4A on an expanded scale is shown in Fig. 4B with the atom labeling given in Fig. 1. It reflects bond-strength distribution over the benzene ring (elements 1 to 6), strong double bond (elements 7 and 8), and weaker single bond (elements 6 and 7) of the vinylene group. This bonding pattern is to be expected from the molecular structure.

We next examine the coordinates Q_ν and momenta P_ν of the dominant electronic oscillators. Vibrational normal modes represent coherent displacements of various atoms, and these electronic modes represent the displacements of the electronic density matrix with respect to $\bar{\rho}$. The diagonal elements reflect induced charges on various atoms, whereas the off-diagonal elements represent dynamical fluctuations of interatomic chemical bonding (*4*–*6*). Our calculations show that the absorption is dominated by five oscillators denoted I to V. The coordinate and momentum eigenvectors of the oscillator responsible for the lowest absorption peak I of $PPV_{(10)}$ are shown in Fig. 4, C and D. The same quantities for the second oscillator corresponding to peak II are shown in Fig. 4, F and G. Despite the different structures of these electronic modes, the delocalization pattern of the off-diagonal elements representing electronic coherence between different atoms is similar. Both modes are delocalized and can be viewed as $d \rightarrow d^*$ transitions. Q_ν and P_ν clearly show that the weak coherences between the phenylene ring of the ith repeat unit, and the vinylene group of the i + 1-st repeat unit are enhanced by optical excitation. In addition, a weak dynamical coherence develops between the ith and the i + 2-nd repeat units. These figures illustrate that finite size effects are limited to the terminating repeat

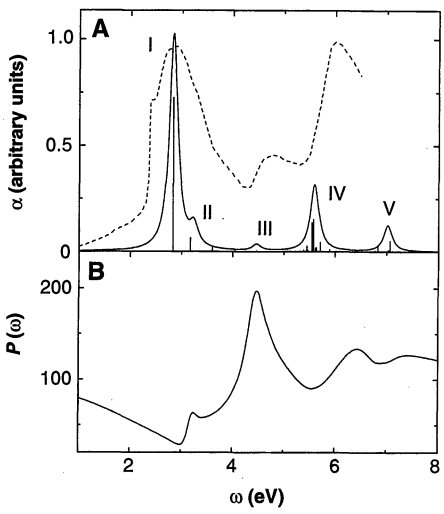

Fig. 3. (**A**) Absorption spectrum of $PPV_{(10)}$ (the imaginary part of α Eq. 1. Dashed line, experimental absorption of a PPV thin film (*24*); solid line, absorption lineshape of $PPV_{(10)}$ obtained with 12 effective modes calculation with linewidth Γ_ν = 0.1 eV. The vertical lines represent oscillator strengths f_ν, $\nu = 1, K^2/4$ of $PPV_{(10)}$ obtained by the full TDHF. (**B**) The frequency-dependent inverse participation ratio of the induced density matrix.

units and that the momenta are more delocalized than the coordinates for a single unit. The coherence size, that is, the "width" of the momentum density matrix along the coordinate axes, where the coherences decrease to 10% of their maximum values, is five repeat units. The same modes for a longer chain [$PPV_{(20)}$] displayed in Fig. 4, E and H, are virtually identical to those of $PPV_{(10)}$. Therefore, 10 repeat units already resemble the infinite chain as far as the optical spectrum is concerned.

The coordinate and momentum of peak III of $PPV_{(10)}$ are shown in Fig. 5, A and B. This mode is delocalized with a coherence size similar to modes I and II; however, its structure along the oligomer chain is very different—bonding is weak at the center and strong toward the edges. The electronic modes are most suitable for investigating charge transfer processes and photoconductivity (*28*, *29*). The strong local optical dipoles along the chain can affect charge transfer and electron hopping. Oscillator III, which has the strongest optical coherences induced at the chain ends (see Figs. 5A and 4B), should play an important role in effects involving charge separation.

The coordinates and momenta of the high-frequency peaks IV and V of $PPV_{(10)}$ (Fig. 5, D, E, G, and H) are completely localized on a single-repeat unit. This behavior is markedly different from polyacety-

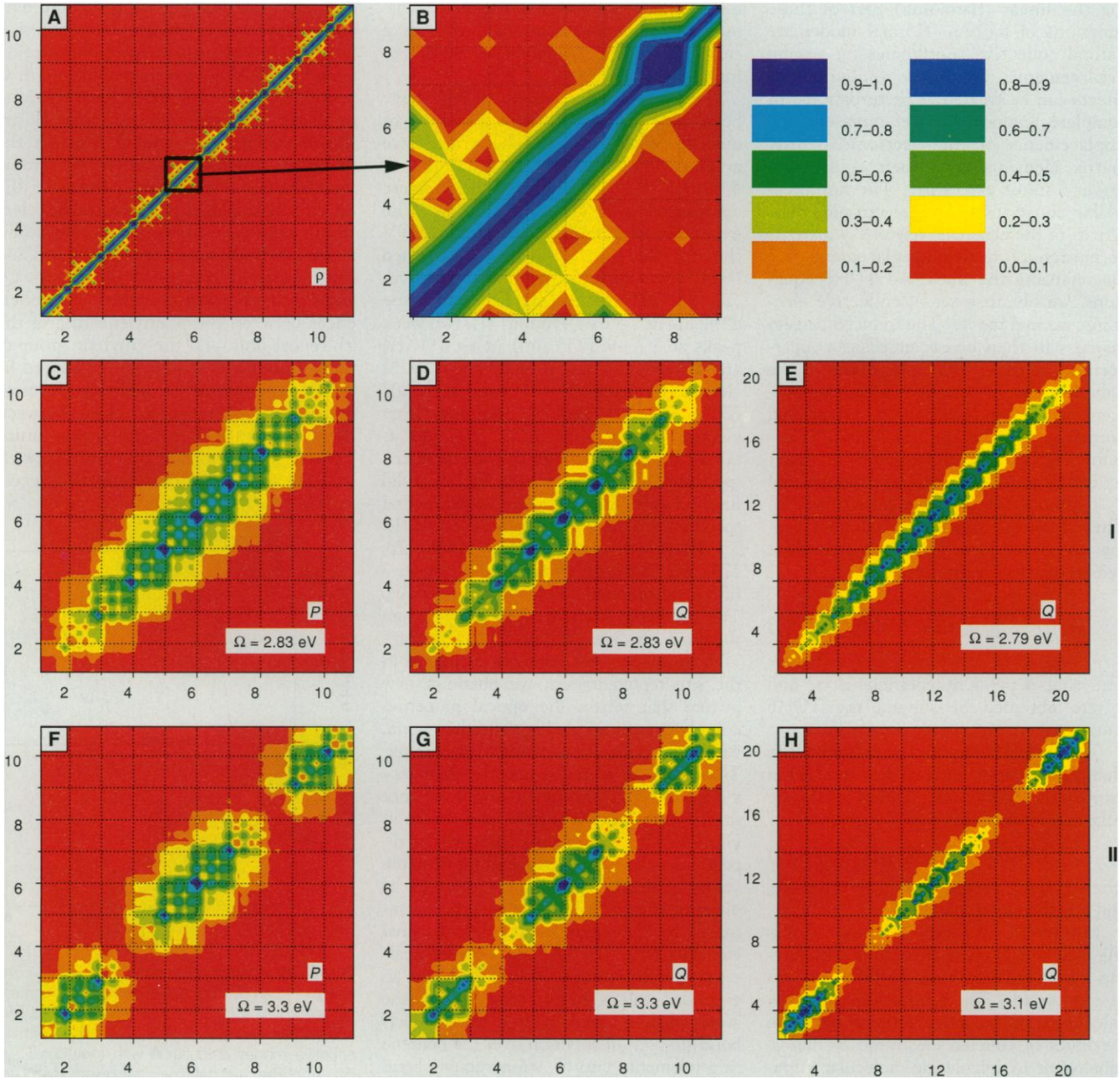

Fig. 4. Contour plots of density matrices. (**A**) $\bar{\rho}$ of $PPV_{(10)}$; (**B**) magnified region of (A) representing the single unit of polymer chain and the color maps; (**C**) momentum and (**D**) coordinate of $PPV_{(10)}$, and (**E**) coordinate of $PPV_{(20)}$ of the lowest absorption peak I, (**F**, **G**, and **H**) are the same quantities as in (C) to (E), but for the second absorption peak (II). The axis labels represent the repeat units, except in (B) where the axes represent the individual carbon atoms as numbered in Fig. 1.

lene, where the electronic coherence size increases monotonically for the higher frequency modes (Fig. 2) (5). The coordinates of these modes for a single PPV unit on an expanded scale are shown in Fig. 5, F and I. For peak IV the optically induced coherences only involve the phenylene ring carbon atoms 1, 2, 4, and 5 (Fig. 1), in agreement with the results obtained in (26, 28). The oscillator responsible for peak IV represents several nearly degenerate localized oscillators (Fig. 3A). The high-frequency peak V predicted by our calculations lies beyond the experimentally studied frequency range. It corresponds to localized and weakly delocalized transitions involving the vinylene group atoms 7 and 8, and the phenylene ring atoms 3 and 6. A weak coherence between the vinylene groups of neighboring repeat units is observed as well.

Even though the CEO approach is eigenstate-free, it is instructive to establish its connection to the more traditional eigenstate representation. The νth oscillator represents the optical transition between the ground state ψ_g and the νth excited state ψ_ν. The matrices representing the coordinate Q_ν and momentum P_ν are given by $(Q_\nu)_{mn} = \langle\psi_\nu|c_m^+c_n|\psi_g\rangle + \langle\psi_g|c_m^+c_n|\psi_\nu\rangle$, $(P_\nu)_{mn} = \langle\psi_\nu|c_m^+c_n|\psi_g\rangle - \langle\psi_g|c_m^+c_n|\psi_\nu\rangle$. Q_ν and P_ν thus carry considerably reduced information about the global eigenstates $|\psi_\nu\rangle$. A different perspective on these modes is obtained by expanding them in the molecular orbital representation using a basis set of pair molecular orbital pairs. Let us denote

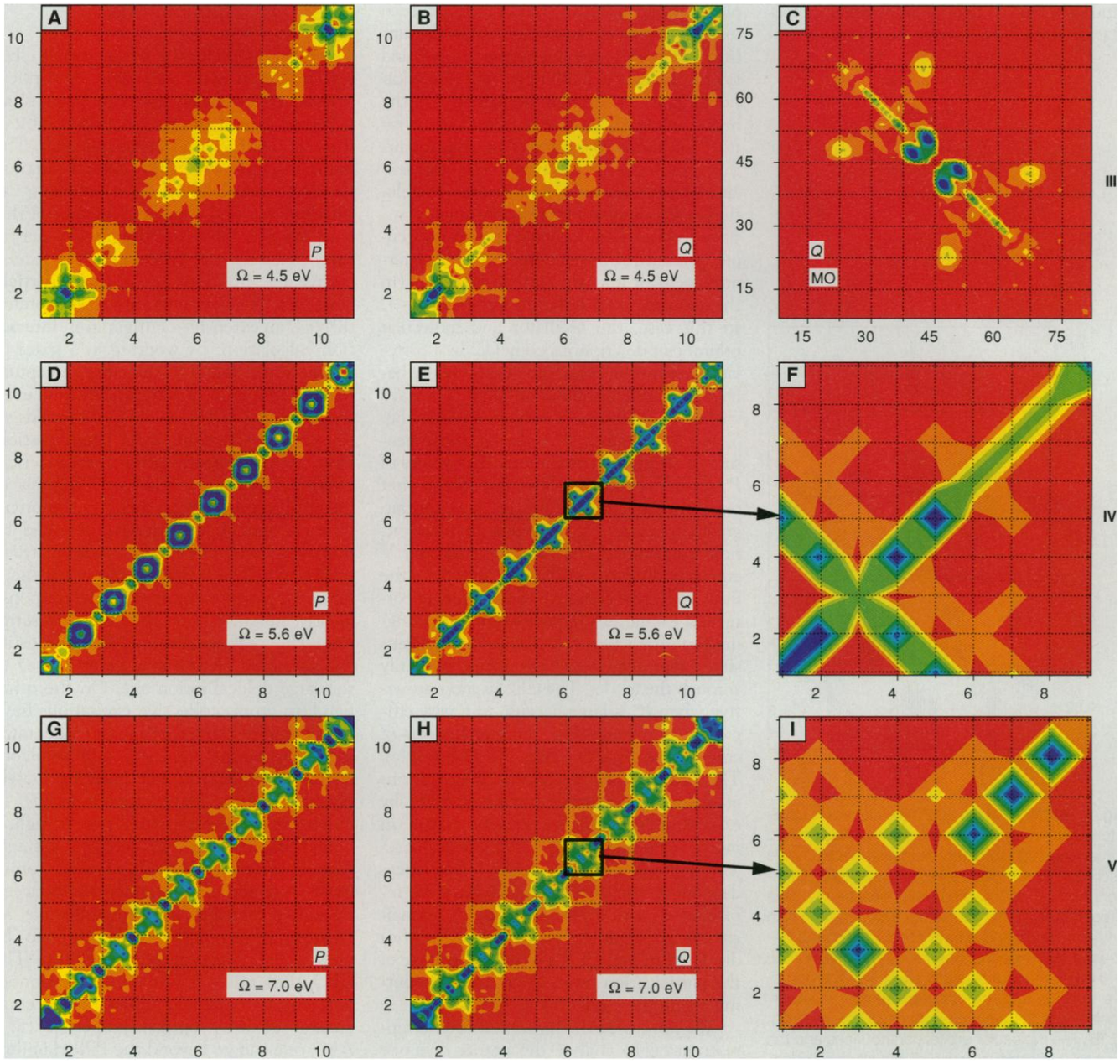

Fig. 5. Contour plots of density matrices. (**A**) Momentum and (**B**) coordinate in the real-space and (**C**) coordinate in the molecular orbital (MO) representation of peak III of $PPV_{(10)}$. (**D**) Momentum and (**E**) coordinate of $PPV_{(10)}$ for absorption peak IV, and (**F**) magnified area of (E) representing the single unit of polymer chain. (**G**, **H**, and **I**) The same quantities as in (B) to (F) but for absorption peak V. The axes of (A), (B), (D), (E), (G), and (H) represent the repeat units of polymer chain. The axes of (C) denote the molecular orbitals. The axes in (F) and (I) represent the number of carbon atoms.

the creation and annihilation operator for the ith molecular orbital as c_i^+ and c_i, respectively. We then have

$$Q_\nu = \sum_{i,j}^{N^2/4} \alpha_{i,j}^\nu (c_i^+ c_j + c_j^+ c_i) \quad (5)$$

where i runs over initially unoccupied orbitals (particles) and j denotes occupied orbitals (holes) (Fig. 6A). The coefficients, α normalized as $\sum_{i,j} |\alpha_{i,j}^\nu| = 1$, represent the contribution of the $j \rightarrow i$ transition to the νth oscillator. Note that the indices n, m used earlier represent localized atomic orbitals whereas i, j denote delocalized molecular orbitals. To illustrate how various molecular orbitals contribute to our five dominant electronic modes, we have introduced the following two quantities

$$R^\nu(j) = \sum_i [\alpha_{i,j}^\nu]^2 \text{ and } P^\nu = \frac{1}{\sum_{i,j} [\alpha_{i,j}^\nu]^2} \quad (6)$$

where $i, j = 1, \ldots, N/2$, and $\nu = \text{I}, \text{II}, \ldots, \text{V}$. $R^\nu(j)$ represents the total contribution of the jth molecular orbital to all orbital pairs appearing in the νth oscillator. $R^\nu(j)$ for the five dominant oscillators in $PPV_{(10)}$ are displayed in Fig. 6B. $R^I(j)$ is relatively localized in the vicinity of the HOMO-LUMO transition (between the highest occupied and lowest unoccupied orbitals), whereas additional pairs of orbitals contribute to the higher modes. The inverse participation ratio P^ν measures the number of orbital pairs that contribute significantly to the νth oscillator. In the absence of electronic correlations, each oscillator represents a single transition between an occupied and an unoccupied orbital (in the quantum chemistry terminology) or a single particle-hole pair (in the semiconductor terminology) and $P^\nu = 1$. In this case, the oscillator and molecular orbital pair descriptions coincide. In a correlated electronic structure, each mode becomes a linear combination (that is, a wave packet) of orbital pairs as represented by Eq. 5, and P^ν increases. P^ν is thus a useful measure of electronic correlations. The values of P^ν given in Fig. 6B show that the higher oscillators are more collective and contain gradually increasing numbers of electron-hole pair states. The oscillators III and V corresponding to $d \rightarrow l^*$ transitions have the most collective character. Such strongly correlated excitations require extensive configuration-interaction calculations in an eigenstates approach. Here they appear naturally through the modes. The CEO is most attractive when P^ν is large because in a very efficient way it lumps the important effects of correlations directly into the observables. The collective nature of optical excitations at different frequencies can be analyzed by expanding the induced density matrix in molecular orbitals $\delta\rho(\omega) = \sum_{i,j} \alpha_{i,j}(\omega)(c_i^+ c_j + c_j^+ c_i)$. We can then define a frequency-dependent participation ratio $P(\omega)$ by replacing $\alpha_{i,j}^\nu$ with $\alpha_{i,j}(\omega)$ in Eq. 6. (A normalization $\sum_{i,j} |\alpha_{i,j}(\omega)| = 1$ is assumed). $P(\omega)$ displayed in Fig. 2B is a weighted average of the participation ratios P^ν of the contributing electronic oscillators.

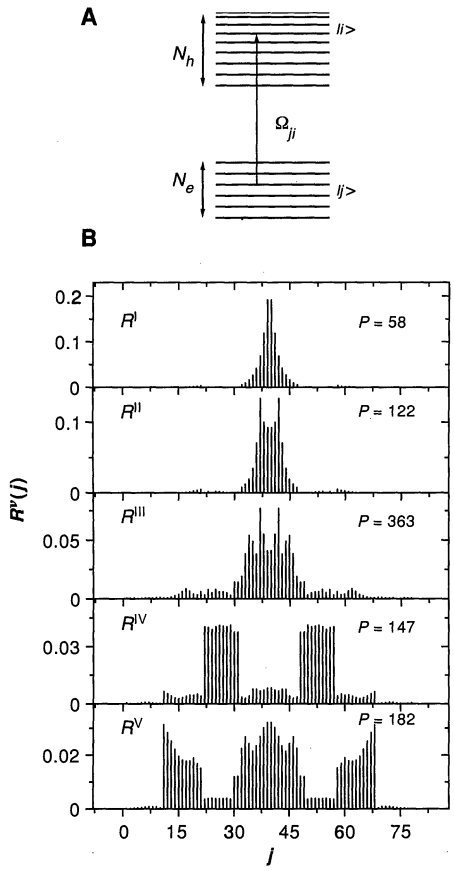

Fig. 6. (**A**) Origin of the collective electronic oscillators. Each transition between an occupied and an unoccupied orbital represents an electron-hole oscillator. In a molecule with N_e occupied (electron) and N_h unoccupied (hole) orbitals we have altogether $N_e \times N_h$, oscillators. For a system with a filled valence and empty conduction band described by a "minimal basis set," $N_e = N_h = N/2$, and the number of oscillators is $N^2/4$. The collective oscillators Q_ν can be represented as superpositions of the electron-hole oscillators (see Eq. 7). (**B**) The molecular orbital contributions and the inverse participation ratios of orbital pairs corresponding to the five dominant modes of $PPV_{(10)}$ absorption. The inverse participation ratio P^ν measures the effective number of electron-hole pairs contributing to a given collective oscillator.

We have used the molecular orbital representation to analyze the nature of mode III. Its coordinate in the molecular orbital representation is shown in Fig. 4C. The figure clearly shows that only a few molecular orbitals close to HOMO-LUMO contribute to this transition. The strongest orbitals can be identified as either delocalized or localized, and mode III corresponds to $l \rightarrow d^*$ and $d \rightarrow 1^*$ transitions. Our calculations further show that the frequencies of modes I, II, and III are red-shifted and gradually saturate with increasing chain length, whereas the frequencies of modes IV and V are not affected by size. These findings are consistent with the delocalized and localized nature of the two groups of modes respectively as displayed in Figs. 4 and 5.

Discussion and Other Applications

The main reason for the success of the CEO representation is the following. An optical excitation moves an electron from some occupied orbital to an unoccupied orbital, thereby creating an electron-hole pair. The natural description of the optical response should therefore be based on following the simultaneous and coupled dynamics of this pair; the two indices of the density matrix carry precisely this information. Molecular eigenstates, however, use a single-particle basis set. Correlations are incorporated through an extensive configuration interaction calculation. By working in a space of higher dimensionality (the pair) we capture the essential physics of the system, and even the simplest (TDHF) factorization yields an adequate description. In a single-particle basis, a much more extensive numerical effort is needed. A real-space analysis of linear absorption that pinpoints the origin of each optical transition is obtained by displaying the electronic mode matrices graphically. The fact that only a few oscillators typically dominate the response greatly simplifies the theoretical description. The weak anharmonicities that justify the harmonic picture may be attributed to the large delocalization size. On the other hand, in atoms collective excitations have been found to converge to local modes rather than to normal modes (*30*). In semiconductors, the electron-hole pairs are loosely bound and form Wannier excitons (*3*). In molecular aggregates, each pair is tightly bound and can be considered as a single particle (Frenkel exciton) (*31, 32*). Conjugated polymers are intermediate between these two extremes, and the collective oscillators in conjugated polymers can be viewed as charge-transfer excitons. The CEO thus offers a unified description of different materials and allows a direct comparison of their optical properties (*33*). Also, one can go beyond the PPP Hamiltonian and the TDHF approximation and include additional variables and use a different ansatz for the wave function (*34*). Technically the calculation of optical prop-

erties with summation over states is also unified and universal. However, very different approximate schemes and terminologies are usually used in the calculation of the eigenstates of various systems, prohibiting a clear comparison and obscuring the origin of differences. The electronic oscillator picture applies to all materials by simply changing parameters (such as the electron hole mass, the Coulomb interaction, and the hopping matrix elements) (*35*).

We next review the computational advantages of the electronic oscillator approach. The sum-only states method becomes rapidly more expensive with molecular size. Both calculating the eigenstates and performing the necessary summations over them are intractable for large systems. Knowing the complete set of eigenstates allows the calculation of any optical response including to strong fields. This is therefore an "all or nothing" approach. The oscillator approach carries less information but for considerably less effort. Computational time of configuration interaction calculations scales as N^6; the CEO procedure scales only as N^2. Our results allow the interpretation of the most interesting crossover region toward the bulk.

The significance of the oscillator picture is even more pronounced when nonlinear optical properties are calculated (*4*, *5*). Interference effects in the sum-over-states approach result in an almost complete cancellation of large positive and negative contributions to optical susceptibilities (*36*, *37*), which limits the accuracy and makes approximate calculations dangerous (because innocent approximations may lead to huge errors). One consequence of this is that individual terms do not have the correct scaling with size. The latter is only obtained once all of the terms are carefully combined. In the oscillator picture these cancellations are built in from the start and each separate contribution to the susceptibility scales properly. The present discussion focuses on the resonant response. However, the real-space approach has been shown to provide an adequate description of the scaling and saturation of off-resonant linear and nonlinear polarizabilities (*4*, *5*).

We further note that by treating the electronic degrees of freedom as oscillators we can couple them more naturally to nuclear degrees of freedom, which constitute another set of oscillators. The incorporation of nuclear notions thus becomes much more straightforward compared with the eigenstate representation and lends itself more easily to semiclassical approximations.

The oscillator approach allows us to develop a natural framework for the interpretation and the design of molecules with specific properties. Instead of asking which of the many-electron states are most relevant, we can explore how different regions of the molecule couple and affect each other. We can translate $\delta\rho(t)$ into a nonlocal response function $\alpha_{nm}(t)$, which shows how the interaction with a field at point n affects the polarization at point m (*38*). The total polarizability is given by summing this quantity over n and m $\alpha(t) = \Sigma_{nm}\, \alpha_{nm}(t)$. The nonlocal character of the response is intimately connected with the electronic coherence of the induced density matrix. One can then address directly the effects of donor-acceptor substitutions and geometry.

Electronic motions may now be probed directly on the femtosecond time scale and the nanometer length scale by nonlinear spectroscopic techniques. This has been recently demonstrated in semiconductor quantum wells (*39*), single-molecule spectroscopy (*40*–*42*), and Rydberg atoms (*43*). The CEO approach should allow us to analyze the temporal and spatial microscopic dynamics underlying energy and electron transfer processes in substituted conjugated molecules by using real-space wave packets representing the single-electron density matrix. A physical picture for coherent versus incoherent electron transfer processes can then be developed in terms of off-diagonal or diagonal pathways, respectively, of the electronic density matrix.

The CEO is conceptually similar to density functional theory, which aims at calculating the ground state with an energy function that depends only on the charge density, that is, the diagonal elements of the density matrix in a localized basis (*44*). The CEO is a natural extension of density functional theory that includes the electronic coherences contained in off-diagonal elements. These carry the key information about electronic excitations and allow the calculation of spectra with only ground-state information.

REFERENCES AND NOTES

1. G. Herzberg, *Electronic Spectra of Polyatomic Molecules* (Van Nostrand, Toronto, Canada, 1966).
2. J. F. Ward, *Rev. Mod. Phys.* **37**, 1 (1965); B. J. Orr and J. F. Ward, *Mol. Phys.* **20**, 513 (1971).
3. H. Haug and S. W. Koch, *Quantum Chemistry of the Optical and Electronic Properties of Semiconductors* (World Scientific, Singapore, 1990).
4. S. Mukamel, A. Takahashi, H. X. Wang, G. Chen, *Science* **266**, 250 (1994); V. Chernyak and S. Mukamel, *J. Chem. Phys.* **104**, 444 (1996).
5. S. Tretiak, V. Chernyak, S. Mukamel, *Chem. Phys. Lett.* **259**, 55 (1996).
6. T. Wagersreiter and S. Mukamel, *J. Chem. Phys.* **104**, 7086 (1996).
7. H. A. Lorentz, *The Theory of Electrons* (Dover, New York, 1952); L. Rosenfeld, *Theory of Electrons* (North-Holland, Amsterdam, 1951).
8. U. Fano, *Rev. Mod. Phys.* **45**, 553 (1974).
9. E. B. Wilson, J. C. Decius, P. C. Cross, *Molecular Vibrations* (McGraw-Hill, New York, 1955).
10. R. W. Hellwarth, *Progr. Quant. Electron.* **5**, 2 (1977); B. J. Berne and R. Pecora, *Dynamic Light Scattering* (Wiley, New York, 1976).
11. S. Mukamel and H. X. Wang, *Phys. Rev. Lett.* **69**, 65 (1992).
12. H. Fukutome, *J. Mol. Struct. Theochem.* **188**, 337 (1989), and references therein.
13. R. McWeeny and B. T. Sutcliffe, *Methods of Molecular Quantum Mechanics* (Academic Press, New York, 1976); E. R. Davidson, *Reduced Density Matrices in Quantum Chemistry* (Academic Press, New York, 1976); A. Szabo and N. A. Ostlund, *Modern Quantum Chemistry* (McGraw-Hill, New York, 1989).
14. R. S. Milliken, *J. Chem. Phys.* **23**, 1833 (1955).
15. D. Chandler, *Introduction to Modern Statistical Mechanics* (Oxford Univ. Press, New York, 1987).
16. P. O. Lowdin, *Phys. Rev.* **97**, 1474 (1955); *Adv. Phys.* **5**, 1 (1956).
17. A. E. Reed, L. A. Curtiss, F. Weinhold, *Chem. Rev.* **88**, 899 (1988); A. E. Reed, R. B. Weinstock, F. Weinhold, *J. Chem. Phys.* **83**, 735 (1985).
18. P. Ring and P. Schuck, *The Nuclear Many-Body Problem* (Springer-Verlag, New York, 1976).
19. S. Tretiak, V. Chernyak, S. Mukamel, *Phys. Rev. Lett.* **77**, 4656 (1996).
20. T. W. Hagler, K. Pakbaz, K. F. Voss, A. J. Heeger, *Phys. Rev. B* **44**, 8652 (1991).
21. D. D. C. Bradly, R. H. Friend, H. Lindenberger, S. Roth, *Polymer* **27**, 1709 (1986); D. A. Halliday *et al.*, *Synth. Met.* **55–57**, 954 (1993).
22. A. Sakamoto, Y. Furukawa, M. Tasumi, *J. Chem. Phys.* **96**, 1490 (1992); *ibid.*, p. 3870.
23. B. Tian *et al.*, *ibid.* **95**, 3191 (1991); B. Tian, G. Zerbi, K. Müllen, *ibid.*, p. 3198.
24. U. Rauscher, H. Bässler, D. D. C. Bradley, M. Hennecke, *Phys. Rev. B* **42**, 9830 (1990).
25. J. L. Bredas, R. R. Chance, R. H. Baughman, R. Silbey, *J. Chem. Phys.* **76**, 3673 (1982).
26. J. Cornil, D. Beljonne, R. H. Friend, J. L. Bredas, *Chem. Phys. Lett.* **223**, 82 (1994).
27. W. Z. Wang, A. Saxena, A. R. Bishop, *Phys. Rev. B* **50**, 6068 (1994).
28. M. Chandross *et al.*, *ibid.*, p. 14702.
29. A. K. Ghosh, D. L. Morel, T. Feng, R. F. Shaw, C. R. Rowe, *J. Appl. Phys.* **45**, 230 (1974).
30. R. S. Berry, in *Structure and Dynamics of Atoms and Molecules: Conceptual Trends*, J. L. Calais and E. S. Kryachko, Eds. (Kluwer, Dordrecht, Netherlands, 1995), pp. 155–181.
31. F. F. So and S. R. Forrest, *Phys. Rev. Lett.* **66**, 2649 (1991); E. I. Haskal, Z. Shen, P. E. Burrows, S. R. Forrest, *Phys. Rev. B* **51**, 4449 (1995).
32. R. van Grondelle, J. P. Dekker, T. Gillboro, V. Sundström, *Biochim. Biophys. Acta* **1187**, 1 (1994); S. E. Bradforth, R. Jimenez, F. von Mourik, R. van Grondelle, G. R. Fleming, *J. Phys. Chem.* **99**, 16179 (1995).
33. B. I. Greene *et al.*, *Science* **247**, 679 (1990).
34. V. M. Axt and S. Mukamel, *Rev. Mod. Phys.*, in press.
35. S. Yokojima, T. Meier, S. Mukamel, *J. Chem. Phys.* **106**, 3837 (1997).
36. S. Mukamel, *Principles of Nonlinear Optical Spectroscopy* (Oxford, New York, 1995).
37. D. C. Rodenberger, J. F. Heflin, A. F. Garito, *Phys. Rev. A* **51**, 3234 (1995); D. C. Rodenberger and A. F. Garito, *Nature* **359**, 309 (1992).
38. T. Wagersreiter and S. Mukamel, *J. Chem. Phys.* **105**, 7995 (1996).
39. S. Weiss *et al.*, *Phys. Rev. Lett.* **69**, 2685 (1992).
40. X. S. Xie and R. C. Dunn, *Science* **265**, 361 (1994).
41. W. P. Ambrose *et al.*, *ibid.*, p. 364.
42. J. K. Trautman *et al.*, *Nature* **369**, 40 (1994).
43. M. Noel and C. R. Stroud Jr., *Phys. Rev. Lett.* **75**, 1252 (1995).
44. R. G. Parr and W. Yang, *Density-Functional Theory of Atoms and Molecules* (Oxford Univ. Press, New York, 1989).

45. Supported by the Air Force Office of Scientific Research, NSF, and the NSF Center for Photoinduced Charge Transfer. T.W. acknowledges the support of the Fonds zur Förderung der Wissenschaftlichen Forschung, Austria, in the form of an E. Schrödinger stipendium (grant number J-01023-PHY). Comments of R. S. Berry are appreciated. The calculations were conducted with the resources of the Cornell Theory Center, which receives major funding from NSF and New York State.